IEEE Access
Multidisciplinary | Rapid Review | Open Access Journal

Received 6 December 2023, accepted 16 January 2024, date of publication 19 January 2024, date of current version 29 January 2024.

Digital Object Identifier 10.1109/ACCESS.2024.3355927

RESEARCH ARTICLE

Quantitative Assessment of Fall Risk in the Elderly Through Fusion of Millimeter-Wave Radar Imaging and Trajectory Features

WEI WANG[1,2], YANXIAO GONG[1,3], HAO ZHANG[1], XIAOLING YUAN[2], (Member, IEEE), AND YUNPENG ZHANG[1]

[1]Suzhou Institute of Biomedical Engineering and Technology, Chinese Academy of Sciences, Suzhou 215163, China
[2]College of Energy and Electrical Engineering, Hohai University, Nanjing 211100, China
[3]Division of Life Sciences and Medicine, School of Biomedical Engineering (Suzhou), University of Science and Technology of China, Hefei 230026, China

Corresponding author: Yunpeng Zhang (zhangyp@sibet.ac.cn)

This work was supported by the Hunan Key Research and Development Program and Guangxi Technology Major Project of China under Grant 2023SK2009 and Grant AA23023005.

This work involved human subjects in its research. Approval of all ethical and experimental procedures and protocols was granted by the Xiangya School of Nursing Ethic Committee of Central South University under Application No. E202108, and performed in line with the Declaration of Helsinki.

ABSTRACT The aging process and chronic diseases can lead to functional decline in older adults, particularly with significant decreases in balance ability, which greatly increases the risk of falls. Traditional balance ability assessment methods typically rely on clinical rating scales, which are subjective and prone to the Hawthorne effect and are difficult to implement for continuous daily assessment. In this paper, we propose a quantitative risk assessment system for elderly falls based on the fusion of millimeter-wave(mmWave) radar imaging and trajectory features. Key features such as the center-of-mass trajectory, trajectory offset, and maximum swing diameter are extracted by improving the fusion clustering algorithm. Then, a model such as Random Forest (RF) is applied to conduct correlation analysis on the features, ultimately proving a significant correlation between feature selection and scale scoring. Subsequently, a quantitative assessment model is established with core algorithms such as Support Vector Regression (SVR), Gradient Boosting Decision Tree (GBDT), Extreme Gradient Boosting (XGBoost), and Light Gradient Boosting Machine (LightGBM) to verify the effectiveness of the evaluation. The result indicates that the LightGBM model achieved the best performance in assessment compared to other models, with a prediction accuracy score of 93.36%. The experiment has demonstrated that the system can effectively capture the features of gait and evaluate early changes in balance ability decline. The research on this system provides a new technological approach to daily fall risk warnings.

INDEX TERMS Millimeter-wave radar, trajectory features, elderly fall, quantitative assessment.

I. INTRODUCTION

The aging of the population has become a common social issue worldwide, and the physical health of older adults has become an enormous challenge for humankind [1], [2]. The World Health Organization has proposed that falls among the elderly seriously threaten their safety, resulting in over 684,000 deaths globally and nearly 37.3 million medical interventions yearly [3]. Timely detection of falls and provision of medical assistance reduces the probability of death and is vital for older adults' physical health and life safety [4]. Therefore, the concept of intelligent, healthy aging has emerged to continuously monitor the fall status of older adults and alert them in time for timely preventive treatment [5].

The traditional medical health assessment model of falls in older adults is based on the clinician's final assessment of medical outcomes, such as clinical scales, according to an

The associate editor coordinating the review of this manuscript and approving it for publication was Szidonia Lefkovits.

outcome-oriented approach, especially in the cause analysis and improvement refinement after a fall event [6], [7], [8]. However, it is difficult to provide a more scientific approach to the physical health of older adults by only observing the outcome of fall events and not focusing on the prior prevention of fall events [9]. Therefore, it is vital to establish an effective quantitative assessment system for fall risk in older adults, which provides a standardized training process through non-contact sensors, objectively records data such as the center of mass trajectory, speed, and pause time during the training process, and uses these data to establish a quantitative assessment model for fall in older adults, which can help the clinicians to more accurately obtain the trend of change in the fall risk of the patients, and propose targeted preventive measures methods, to reduce the probability of fall occurrence [10]. In summary, a sound and improved quantitative fall risk assessment system for intelligent, healthy aging can reduce clinicians' workload for early intervention and risk avoidance [11].

To overcome the above challenges, we propose a quantitative fall risk assessment scheme for older adults based on mmWave radar from Texas Instruments (TI). Combining clinician scale assessment and mmWave radar tracking dynamic trajectory means improving the accuracy of mmWave radar tracking the dynamic trajectory of the human body through the center of mass trajectory based on Doppler frequency shift screening. By tracking the time series of the center of mass, the characteristic parameters of the dynamic balance ability of human movement are extracted and supplemented by scoring according to the clinical scale, and the fall risk assessment model for older adults is established.

The remaining sections of this article are arranged as follows: Section II reviews the related works. Section III discusses the principle and feasibility of using frequency-modulated continuous-wave (FMCW) mmWave radar to obtain human echo signals. Section IV introduces the principle and simulation experiment performance of the proposed method. Section V presents the experiments and feature extraction. Section VI analyzes the results of the experiment and the discussion. Section VII discusses the shortcomings of the current method and future work and research directions. Finally, Section VIII summarizes this article.

II. RELATED WORK

The non-contact fall risk assessment based on mmWave radar has multiple advantages. Firstly, it does not require physical contact and frequent battery replacement compared to wearable sensors [12], [13], [14], [15]. Secondly, it has the advantage of not invading privacy compared to cameras [5]. Thirdly, it has high sensitivity and strong penetrability for moving objects compared to depth sensors such as Kinect [16]. Fourthly, it has the advantages of low cost, small size, and high resolution compared to traditional radar [17]. The most important of the above four benefits is the non-contact data acquisition advantage. Older adults often forget wearable devices, causing assessment interruptions [18]. In addition, wearable sensors may interfere with normal gait walking in older adults. In conclusion, non-contact mmWave radar sensors are suitable for application in remote home monitoring scenarios.

Most falls in older adults are not accidental events but are induced by various risk factors that catalyze each other. To predict older adults' falls, it is vital to incorporate fall-related risk factors and develop solutions for patients in a complete manner [9], [19]. Hosseini et al. [20] developed a multifactorial predictive model for fall risk in hospitalized older adults. The model combines real-time vital signs, motion data, fall history, and muscle strength to identify individuals at high risk for falls in older adults. For data collection, a triaxial accelerometer was used to collect older adults' motion data, which was combined with vital signs for monitoring, while a bidirectional classification model was used to predict fall risk. Model results showed an accuracy of 0.98, a sensitivity of 0.96, and a specificity of 1, achieved in 80 simulated falls and 40 activities of daily living (ADL). The model demonstrated higher accuracy in fall risk prediction than the traditional Morse Fall Scale. Tools to quantify fall risk and assess functional deficits can target people at increased fall risk and tailor a range of improvements to deficiencies to reduce fall rates and decrease fall risk. Greene et al. [21] developed a fall risk assessment method that combines clinical assessment and sensor data to provide a more accurate risk assessment than a single method. 292 community-dwelling older adults were asked to wear inertial sensors, and data were collected using the TUG test. The dataset was segmented by ten-fold cross-validation for dataset segmentation, and the experimental results showed that the combination of clinical and sensor-based methods produced an accuracy of 0.76, compared to 0.736 for sensor-based assessment alone and 0.688 based on clinical risk factors alone. Mishra et al. [22] predicted a 6-month fall risk in 92 older adults using geriatric assessments, GAITRite measurements, and fall history. They found that the Support Vector Machine (SVM) model had the best performance, with an AUC of 0.80, sensitivity of 0.82, specificity of 0.72, and accuracy of 0.75. Zhang et al. [23] developed a gait parameter-based fall risk assessment model for community-dwelling older adults. 46 older adults were asked to wear IMU inertial measurement units on both feet, and the gait spatial-temporal parameters of the subjects were acquired through the gait analysis system of Azure Kinect. The study constructed multiple machine-learning models to assess the fall risk level in older adults. The experimental results show that the K-Nearest neighbor (KNN) performed best among all the models with an accuracy of 0.80 on the individual test set, an F1 score of 0.67, and an area under the receiver operating characteristic curve of 0.83. Gait frequency was the most significant feature associated with fall risk, followed by body mass index and gait cycle variability. The findings suggest that the KNN model can provide a quantitative and objective evaluation of fall risk for older adults

living in the community. The assessment is more accurate when considering gait parameters and disease history.

In the above study, fall risk in older adults was quantitatively assessed primarily through wearable devices and clinical functional tests. However, wearable devices are not easy to promote in practical applications because they must be carried around and lead to discomfort easily caused by irregular wear. There are problems of personal privacy leakage with non-contact cameras. Therefore, in this study, FMCW mmWave radar is utilized to extract the walking trajectory information of the fall risk assessment test for older adults, and human dynamics parameters are extracted by formula conversion, which combined clinical scales and dynamic balance ability characteristic parameters. The above means of data fusion and analysis will be a potential means of fall risk prediction for the application of smart homes for older adults in terms of technology. The research will improve the robustness of the trajectory algorithm, further implement trajectory imaging techniques for older adults in home situations, and ultimately use daily senseless continuous assessment as an alternative to existing scale-based methods for assessing fall risk.

III. OBTAINING HUMAN ECHO SIGNAL BY MMWAVE RADAR

We utilized the Texas Instruments (TI) IWR6843 mmWave radar evaluation board with a linear frequency modulation range of 60-64GHz, consisting of four receive (RX) antennas and three transmit (TX) antennas for collecting point cloud echo signals. Figure 1 shows the workflow diagram of acquiring human body echo signals using the mmWave radar.

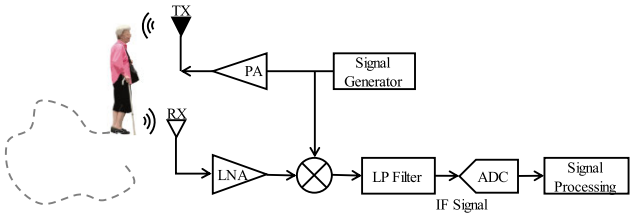

FIGURE 1. mmWave radar workflow diagram.

A. HUMAN ECHO SIGNAL MODELING

The basic architecture of the mmWave radar TX and RX array is shown in Figure 2, with the spacing of two neighboring TX antennas $d_t = 5$mm and two neighboring RX antennas $d_r = 2.5$mm. Assume that human targets are in the mmWave radar detection area, corresponding to a total of scattering points I, where the azimuth of the scattering point i ($i = 1, 2, \cdots, I$) is θ_i.

Frequency-modulated (FM) pulses are generated in the signal generator, amplified by a power amplifier (PA), and transmitted to the outside. The mmWave radar transmits a linear FM pulse, and the TX signal in a sawtooth FM cycle is

$$S_T(t) = A_T \cos\left(2\pi f_0 t + \pi\mu t^2 + \phi(t)\right) \tag{1}$$

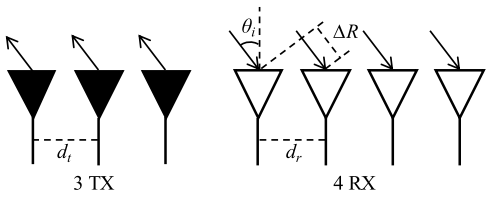

FIGURE 2. mmWave radar transmit and receive array architecture.

where $S_T(t)$ is the TX signal, A_T is its amplitude, f_0 is the starting frequency, $\phi(t)$ is the phase noise, $\mu = B/T_c$ is the slope, B is the chirp bandwidth, and T_c is the ramp period.

The TX signal is transmitted to the outside world through the antenna. The detected object reflects when the electromagnetic wave arrives at a distance of R_i from the radar. The RX signal is obtained as

$$S_R(t) = \sum_{i=1}^{I} A_R \cos\left(2\pi f_0(t - t_{di}) + \pi\mu(t - t_{di})^2 + \phi(t - t_{di})\right) \tag{2}$$

where $S_R(t)$ is the RX signal, A_R is its amplitude, $t_{di} = 2(R_i + v_{di}t)/c = 2R_i/c + f_{di}t/f_0$ is the instantaneous time delay of the RX and TX signals, v_{di} is the velocity of the scattering point i, f_{di} is the Doppler shift of the scattering point i, and R_i is the distance from the radar to the detected object.

The RX signal is mixed with the TX signal with a mixer, which calculates the frequency difference between the TX and RX signals. Two frequency differences are $f_1 = f_T + f_R$ and $f_2 = f_T - f_R$. To reduce the sampling rate, it is known from the Nyquist sampling theorem that the low-pass (LP) filter serves to filter out those unrelated frequency components and the components with the frequency of f_1 are suppressed, so that the baseband signal with the frequency of f_2 enters into the analog-digital converter (ADC).

Based on the above principle, after mixing and LP filtering of the TX signal and RX signal, only the differential frequency component f_2 is retained. And the IF signal phase can be obtained as the phase difference between the TX signal and the RX signal, and the instantaneous phase of IF signal is

$$\begin{aligned}\varphi_{IF}(t) &= \varphi_T(t) - \varphi_R(t) \\ &= 2\pi f_0 t_{di} + 2\pi\mu t_{di} t - \pi\mu t_{di}^2 + \Delta\phi_i(t)\end{aligned} \tag{3}$$

And the IF signal is obtained as

$$S_{IF}(t) = S_T(t)S_R^*(t) = \sum_{i=1}^{I} A_{Ri} e^{j(2\pi f_{bi}t + \phi_{bi}(t) + \Delta\phi_i(t))} \tag{4}$$

where $S_{IF}(t)$ is the IF signal, A_{Ri} is its amplitude, f_{bi} is the frequency difference of the IF signal at the scattering point i, $\phi_{bi}(t) = 2\pi f_0 t_{di} + \pi\mu t_{di}^2$ is the phase at the scattering point i, and $\Delta\phi_i(t) = \phi(t) - \phi(t - t_{di})$ is the residual noise at the target i. Due to the close proximity of the human target to the radar, the values of residual noise $\Delta\phi_i(t)$ and the $\pi\mu t_{di}^2$ term in phase $\phi_{bi}(t)$ are small and negligible.

Therefore, the IF signal can be rewritten as

$$S_{IF}(t) = \sum_{i=1}^{I} A_{Ri} e^{j(2\pi f_{bi} t + 2\pi f_0 t_{di})} = \sum_{i=1}^{I} A_{Ri} e^{j(2\pi \mu t_{di} t + 2\pi f_0 t_{di})} \quad (5)$$

Based on formula (5) and t_{di}, When μ determined, the frequency of the IF signal is constant and the IF signal depends on R_i and f_{di}.

Figure 3 shows the frequency of the three signals as a function of time. Assuming that M linear FM pulses are generated over a period of time, then M IF signals can be obtained, and the number of sampling points during the duration of each linear FM pulse is N. Each column in the two-dimensional matrix at the bottom of Figure 3 represents the sampling points of one frame of the IF signal. The n-th sampling point in the m-th IF signal can be expressed as

$$Y[n, m] = \sum_{i=1}^{I} A_{Ri} e^{j(2\pi n f_{bi} T_f + 2\pi m f_{di} T_s)} \quad (6)$$

where $n = 1, 2, \ldots, N$ is the corresponding marker on the fast time sampling axis, $m = 1, 2, \ldots, M$ is the corresponding marker on the slow time sampling axis, T_f is the sampling interval on the Fast Time Axis, also called the ADC sampling interval, and T_s is the sampling interval on the Slow Time Axis, also called the inter-frame interval (IFI).

B. HUMAN ECHO SIGNAL MODEL ACQUISITION

Compared to traditional pulse radar systems that use periodic emission of short pulses, mmWave radar can continuously emit FM signals and simultaneously measure human target scattering points' coordinates and Doppler information. As shown in Figure 4, the mmWave radar module integrates a radio frequency (RF) front-end, low noise amplifier, advanced RISC machine (ARM) processor, digital signal processing (DSP), memory, and other components, which can satisfy the processing requirements of intermediate frequency sampling buffering, range fast Fourier transformation (Range-FFT), Doppler fast Fourier transformation (Doppler-FFT), angle fast Fourier transformation (Angle-FFT), static clutter filtering, and constant false alarm rate detection (CFAR). The acquisition of point cloud data is of great significance for subsequent analysis of human targets.

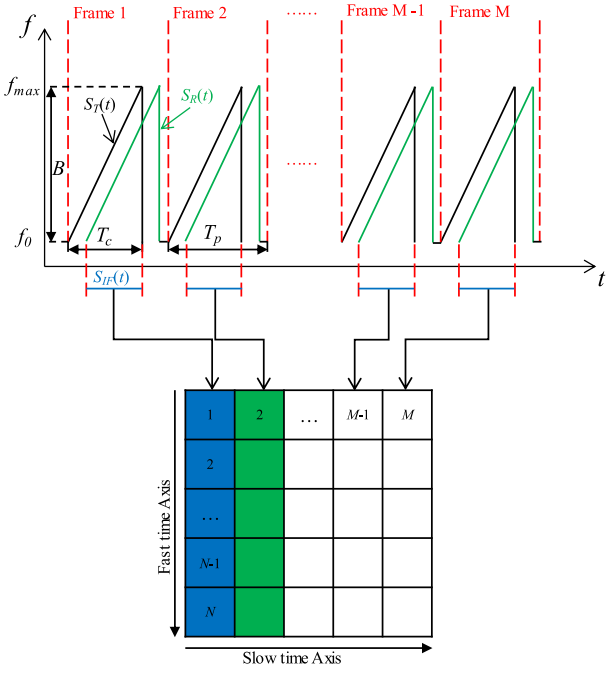

FIGURE 3. mmWave radar signal model.

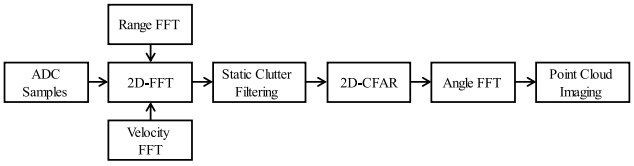

FIGURE 4. Signal processing flow.

1) TWO-DIMENSIONAL FAST FOURIER TRANSFORM (2D-FFT)

Based on the radar sampling data matrix Y shown in the formula (6), the IF signal frequency f_{bi} and Doppler shift f_{di} contain each scattering point's distance and Doppler information. Each column of the radar sampling data matrix Y is processed with N-point FFT to find the distance information of the target, and each row is processed with M-point FFT to find the Doppler information of the target [24]. The processing flow is shown in Figure 5.

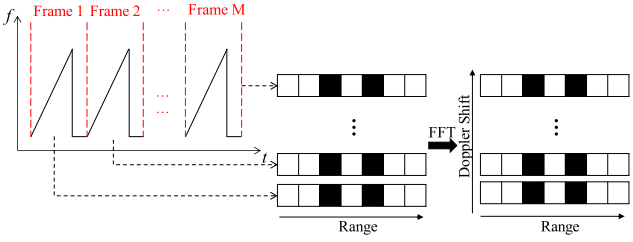

FIGURE 5. 2D-FFT processing flow.

2) STATIC CLUTTER FILTERING

After performing 2D-FFT, it is necessary to perform 3D point cloud imaging of the moving targets. Since the distance from a stationary target to the radar antenna is constant, the time delay of the stationary target on each received pulse is also constant. To remove the static target's point cloud, the mean value needs to be calculated for each distance unit and each antenna and then subtracted from the data to remove the zero-Doppler targets. The above process is known as the phasor-mean cancellation algorithm.

3) CONSTANT FALSE ALARM DETECTION

In crowded environments, the acquisition of human echo signals usually includes various factors such as target information, background noise, and clutter interference. To effectively detect human targets, the CFAR algorithm is employed to filter out clutter scattering points. Subsequently, the CFAR algorithm for distance and Doppler dimension frequency shift of the radar sampling data matrix Y. The CFAR algorithm is shown in Figure 6.

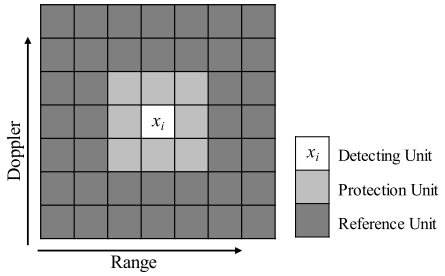

FIGURE 6. CFAR algorithm.

4) PHASE METHOD OF ANGLE MEASUREMENT

For the same scattering point $i(i = 1, 2, \ldots, I)$, its angle can be estimated through the phase difference of the echo signals received by two RX antennas [25]. Assuming that the difference in the signal path between two adjacent receiving antennas is ΔR_i, the phase difference of the RX signal at the time t for the i scattering point can be expressed as

$$\Delta\phi_i(t) = \frac{2\pi\,\Delta R_i}{\lambda} \tag{7}$$

As shown in Figure 2, the difference in the signal path between two neighboring RX antennas can be approximated as follows

$$\Delta R_i = d_r \sin\theta_i \tag{8}$$

Based on formulas (7) and (8), the Angle-FFT extracts the phase information between antennas by simultaneously sampling the signals from multiple RX antennas and utilizing the slight phase differences between the RX signals. Therefore, the azimuth angle θ_i of the scattering point i can be expressed as

$$\theta_i = \sin^{-1}\left(\frac{\lambda\,\Delta\varphi_i(t)}{2\pi\,d_r}\right) \tag{9}$$

Hence, the 3D coordinates of the scattering point i can be expressed as

$$\begin{cases} x_i = R_i\cos(\theta_i)\sin(\varphi_i) \\ y_i = R_i\cos(\theta_i)\cos(\varphi_i) \\ z_i = R_i\sin(\theta_i) \end{cases} \tag{10}$$

where x_i, y_i, and z_i represent the coordinate position of the point i in the 3D space. Therefore, the point cloud data containing the position and Doppler information of the scattering points can be represented by the dataset P_0 as follows

$$P_0 : \{(x_i, y_i, z_i, f_{di}), i = 1, 2, \ldots, I\} \tag{11}$$

IV. PROPOSED METHOD

Based on the above discussion, the method of using mmWave radar for fall risk assessment in older adults generally follows the following steps:

(1) First, the human target position localization is performed based on the radar point cloud data to obtain the position coordinates and Doppler information of all the human body echo signal's point clouds in a single frame state. Second, the spherical coordinate system of the radar point cloud coordinates is transformed into a Cartesian coordinate system. Then, the Density-Based Spatial Clustering of Applications with Noise (DBSCAN) based on Doppler frequency shift extracts the center-of-mass position of the human body in each frame of the point cloud data.

(2) Based on the extended Kalman filter (EKF), the center-of-mass position in each frame is tracked to achieve dynamic trajectory tracking and prediction of the human body.

(3) By tracking the center-of-mass time series, feature parameters of the dynamic balance ability of the human body are extracted. A fall risk assessment model for older adults is established based on clinical scale scores.

The proposed quantitative assessment system framework is shown in Figure 7. For step (1), the human target position detection algorithm, a Doppler frequency shift-based DBSCAN clustering algorithm, is proposed to improve the accuracy of mmWave radar trajectory tracking by clustering the point cloud information in each frame state of mmWave radar point cloud. For step (2), the research proposes an EKF-based human dynamic trajectory prediction algorithm to improve the error generated in the measurement process and realize the tracking of human targets. Finally, for step (3), based on the dynamic trajectory of the mmWave radar, dynamic balance ability feature parameters of the human body are extracted. The accuracy of the quantitative fall risk assessment system is validated by establishing clinical scale scores.

A. DBSCAN CLUSTERING BASED ON DOPPLER FREQUENCY SHIFT

In human dynamic trajectory measurement application scenarios, micro-Doppler effects caused by human breathing, heartbeat, and small-arm swings produce point cloud data with small Doppler frequency shifts. This research proposes a Doppler frequency shift-based clustering method that removes points with small frequency shifts by setting an appropriate Doppler threshold to reduce micro-motion interference on the clustering results, except for the overall translational motion of the human torso.

Clustering methods typically cluster closely spaced points into clusters, with one cluster corresponding to one target [26]. Due to the small size and irregular shape of the human target point cloud data set P_0, this research uses

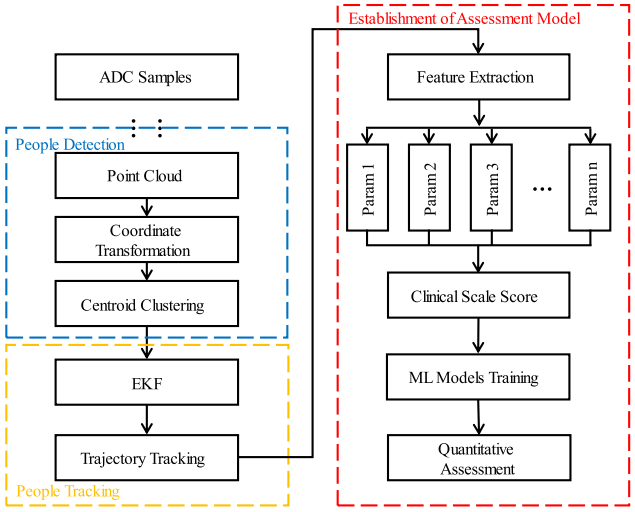

FIGURE 7. A framework for a quantitative fall risk assessment system based on mmWave radar and machine learning algorithms.

the DBSCAN clustering algorithm to extract the center-of-mass feature points of the object and remove unstable noise points in the data. DBSCAN has significant advantages over other clustering algorithms, such as K-means, in the problem of clustering mmWave radar data. Firstly, DBSCAN does not require pre-determination of the number of clusters. Secondly, DBSCAN is a density-based spatial clustering algorithm that can detect clusters of arbitrary shapes. In addition, DBSCAN can identify unstable noise points in the data.

The core parameters of DBSCAN clustering based on the Doppler shift include the cluster radius ε, the minimum number of points n within the cluster radius, and the Doppler threshold f_t. Based on the point cloud set P_0 before clustering in formula (11), the point cloud set P_1 with the Doppler shift less than the Doppler threshold removed is

$$P_1 : \left\{ \left(x_j, y_j, z_j, f_{dj}\right) \mid \left|f_{dj}\right| > f_t, j = 1, 2, \ldots, J \right\} \tag{12}$$

where f_{dj} is the Doppler shift of the point target j, and J represents all the scattering points that satisfy $\left|f_{dj}\right| > f_t$. The processed point cloud set P_1 is clustered using the DBSCAN algorithm to find the cluster centroid as the center-of-mass feature point of the single-frame human target point cloud.

Figure 8 shows the results of the traditional DBSCAN and DBSCAN clustering methods based on Doppler frequency shift filtering for a single frame of human target 3D point cloud data. While the traditional DBSCAN method results in invalid target points after clustering, this method filters out the scattered points with small frequency shifts of human micro-motion in the case of single-frame targets, making the DBSCAN clustering more accurate.

B. EKF ALGORITHM BASED ON HUMAN DYNAMIC TRAJECTORY PREDICTION

With the human body uniform motion model, it is assumed that the target velocity for this model is constant over the

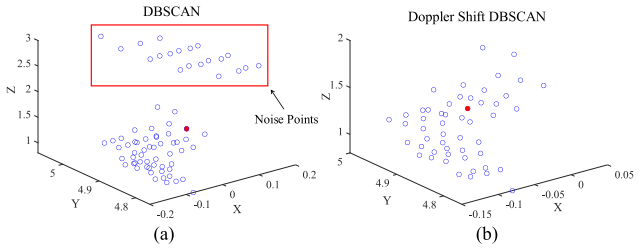

FIGURE 8. Point cloud clustering. (a) Traditional DBSCAN clustering. (b) DBSCAN clustering based on Doppler frequency shift screening.

measurement interval. During measurement, the mmWave radar is subject to bias due to the sensor's performance and environmental disturbances. For example, a jump in target position and a target loss occurs when measuring the same target. To address the above issues, this research uses the EKF algorithm to improve the errors arising during the measurement process. The EKF algorithm consists of a recursive, iterative operation divided into prediction and update steps.

1) PREDICTION STEPS

The target is modeled using a constant acceleration model in conjunction with the actual motion of the mmWave radar target. The target object is viewed as a center-of-mass point. Without considering the size and shape of the center-of-mass point, the focus is on the target object's position, velocity, and acceleration information in mmWave radar Cartesian coordinates. From this, the feature vectors of the model are defined as

$$X_k = (p, v, a)^{\mathrm{T}} = \left(p_x, p_y, v_x, v_y, a_x, a_y\right)^{\mathrm{T}} \tag{13}$$

where X_k is the system feature vector, p_x and p_y are the positions of the target in the Cartesian coordinate system in the X and Y directions (m), v_x and v_y represent the velocity of the target's motion in the X and Y directions(m/s), a_x and a_y represent the acceleration of the target in the X and Y directions(m^2/s).

Based on the constant acceleration model to represent the target motion law, the state transfer matrix A of the constant acceleration model is obtained as

$$A = \begin{bmatrix} 1 & 0 & \Delta t & 0 & \frac{1}{2}\Delta t^2 & 0 \\ 0 & 1 & 0 & \Delta t & 0 & \frac{1}{2}\Delta t^2 \\ 0 & 0 & 1 & 0 & \Delta t & 0 \\ 0 & 0 & 0 & 1 & 0 & \Delta t \\ 0 & 0 & 0 & 0 & 1 & 0 \\ 0 & 0 & 0 & 0 & 0 & 1 \end{bmatrix} \tag{14}$$

where Δt is the two detection sampling intervals. In the prediction step of the EKF algorithm, the priori estimated state vector X_k^- at the current moment can be obtained from the posterior estimated state vector X_{k-1}^+ at the previous moment as

$$X_k^- = AX_{k-1}^+ \tag{15}$$

The prior estimated covariance matrix P_k^- for the current moment is derived from the posterior estimated covariance matrix P_{k-1}^+ for the previous moment as

$$P_k^- = AP_{k-1}^+ A^T + Q^* \tag{16}$$

where Q^* is the covariance matrix of the process noise.

2) UPDATE STEPS

The measurements in each frame have a corresponding target orbit to associate. The association process requires a distance metric calculated from the distance between the measured and the predicted trajectory's center of mass. The measurements are assigned to the closest orbit. Each track's center of mass of all measurements is calculated as the target position. Due to the limited angular resolution of the mmWave radar for boundary detection, the shape of the target is modeled as a point.

For measurements that are not associated with other tracks, a new trajectory is initialized for them if the signal-to-noise ratio of the measurement is sufficiently dense and strong enough. The corresponding trajectory is deleted for trajectory not associated with any measurement.

Finally, the EKF update step is used to estimate the state and covariance of the pedestrian. Due to the nonlinearity of the measurement model, the relationship between state and measurement must be approximated by a Taylor series expansion. The mmWave radar output measures the relative distance, relative azimuth, and relative velocity of the target, thus defining the measurement vector u_k of the EKF algorithm as

$$u_k = (r, \varphi, v)^{\mathrm{T}} \tag{17}$$

where γ represents the relative distance, φ represents the relative azimuth, and v represents the relative velocity. Therefore, the state observation mapping relationship H can be defined as

$$H = \begin{bmatrix} \sqrt{p_x^2 + p_y^2} \\ \tan^{-1}(p_x/p_y) \\ \frac{p_x v_x + p_y v_y}{\sqrt{p_x^2 + p_y^2}} \end{bmatrix} \tag{18}$$

From this, the Kalman gain K_k for the update step can be deduced as

$$K_k = P_k^- C^T \left(z_k^-\right) \left[C\left(z_k^-\right) P_k^- C^T \left(z_k^-\right) + R\right] \tag{19}$$

where C is the first-order partial derivative of the state observation mapping matrix H, z_k is the systematic observation vector, and R is the systematic observation noise. The system measurement residuals t_k are calculated as follows

$$t_k = u_k - H\left(z_k^-\right) \tag{20}$$

Calculate the posterior state vector X_k^+, covariance P_k^+ as

$$X_k^+ = X_k^- + K_k t_k \tag{21}$$

$$P_k^+ = P_k^- - KC\left(X_k^-\right) P_k^- \tag{22}$$

where K is the extended Kalman gain matrix for the updated part of the measurement at the moment k.

For the subsequent human dynamic balance assessment modeling, the Z-axis is omitted to convert the 3D tracking results into 2D tracking results. However, an additional height dimension is introduced in the tracking process, facilitating the increased number of detected features. Therefore, the tracking performance is improved compared to the 2D tracking model.

C. DEVELOPING A RISK ASSESSMENT MODEL FOR FALLS IN OLDER ADULTS

The quantitative assessment system for fall risk in older adults walking at home is shown in Figure 9. During the data collection phase, we establish a mmWave radar-based system for collecting walking trajectory data of older adults to obtain their kinematic parameters. Then, we use a clinically common dynamic balance ability test scale to score the balance ability function of older adults during walking and use the scale score as the label for the dataset. Finally, we extract eight features from the data and use four machine learning algorithms to establish a quantitative assessment model for older adults' fall risk.

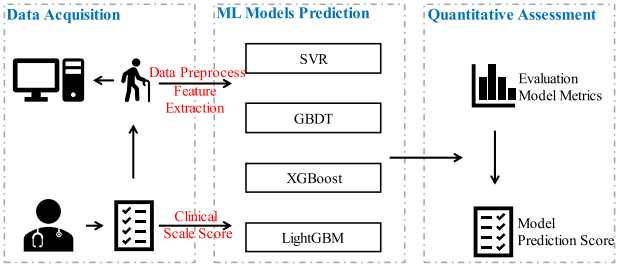

FIGURE 9. Quantitative fall risk assessment model for elderly.

During the data collection phase, the participants perform the balance ability evaluation task in a laboratory setting. TI IWR6843 measures various 2D spatial kinematic parameters of the participants. The software controlled by the host computer provides real-time trajectory parameters for the participants. The collected data are sent to the host computer-based control software. To avoid the impact of subjective factors on the clinical score, three different raters rate the subjects' dynamic balance ability according to the clinical assessment scale, and the average of the three scores is used as the final score.

This research recruits 32 participants to participate in the experiment. Each participant needs to complete eight trajectory tracking tasks divided into forward and backward walking to eliminate the influence of walking habits. The sample size of the experimental dataset is 256. This research selects the RF algorithm and the Pearson correlation analysis to determine the feature vector and the SVR, GBDT, XGBoost, and LightGBM models as supervised regression prediction algorithms to establish the quantitative assessment model. The centroid trajectory, trajectory offset, and max-

imum sway diameter are used as the inputs to the model, and the best model is obtained by extracting the feature parameters for prediction. The reasons for selecting the above four algorithms are that their generalization and nonlinear mapping abilities are good, and the sample size of this study's dataset is small [27].

During the quantitative assessment phase, the participants complete the evaluation task, and their kinematic data on balance ability are collected by sensors and transmitted to a computer. The model's predicted scores for dynamic balance ability are obtained by preprocessing the data and training the model, enabling quantitative assessment of human dynamic balance ability.

Random forest (RF) is a classification and regression technique with simple implementation and low computational overhead, which is suitable for modeling nonlinear data and correlation analysis of variables. Many scholars have used random forest methods for feature selection [28].

Gradient boosting decision tree (GBDT) is a decision tree algorithm constructed based on iterations. It can make both regression and classification predictions, using the classification and regression trees (CART) model as a weak learner, building the new learner in the direction of the gradient decline of the loss function of the previous learner, and training the model through continuous iteration. In the iterative process, residuals exist between the predicted and actual values in each round, and the predictions are made again in the next round based on the residuals. Finally, all the predictions are summed up as the conclusion. Therefore, the additive model of the decision tree of GBDT can be represented as

$$f_m(x) = \sum_{m=1}^{M} T\left(x, \theta_m\right) \tag{23}$$

where $T\left(x, \theta_m\right)$ is the decision tree, θ_m is the decision tree parameter, and M is the number of trees. According to the forward step-by-step algorithm, the step model m is

$$f_m(x) = f_{m-1}(x) + T\left(x, \theta_m\right) \tag{24}$$

Setting y_i as the actual value of the sample i, $f_m(x_i)$ as the predicted value of the sample i,and taking the loss function as the squared loss, the loss function and the minimization loss function of the parameter θ_m as

$$L\left(y_i, f_m\left(x_i\right)\right) = \frac{1}{2}\left(y_i - f_m\left(x_i\right)\right)^2 \tag{25}$$

$$\hat{\theta}_m = \arg\min \sum_{i=1}^{M} L\left(y_i, f_{m-1}(x) + T\left(x; \theta_m\right)\right) \tag{26}$$

Several iterations of the regression tree update the above equation to obtain the final model. LightGBM is an improved model proposed by Microsoft in 2017 based on the GBDT framework [29]. It uses a histogram-based segmentation algorithm instead of the traditional pre-sorted traversal algorithm, which not only outperforms GBDT in terms of training speed and space efficiency but also effectively prevents overfitting and is more suitable for training data.

V. EXPERIMENTS AND FEATURE EXTRACTION

A. EXPERIMENTAL SETUP

The IWR6843 is used for data acquisition, which has a carrier frequency of 60GHz-64GHz, equipped with four RX antennas and three TX antennas, and the parameters are set as shown in Table 1. IWR6843 supports a 120° view angle in both horizontal and vertical directions. Due to the experimental scene top-hung radar evaluation board, the maximum measurement distance is 6m. The sampling frequency is generally selected above 2000 KSPS, where KSPS (kilo sample per second) is the sampling frequency unit, indicating the number of species sampled per second.

TABLE 1. Radar parameters.

Parameter	Value
Start Frequency	61.2GHz
ADC Start time	17μs
Ramp End time	50μs
Frequency Slope	55.27MHz/μs
ADC Samples	64
Band Width	1768.66MHz
ADC Sampling time	32μs
Frame Periodicity	120 ms
ADC Sampling Frequency	2000KSPS

The experiment is conducted in a closed room with experimental equipment including a TI IWR6843 mmWave radar evaluation board (hanging height 2.8m), a computer with MATLAB R2021b (CPU R7-5800H 3.2GHz 16GBRAM), and an intelligent tracking trolley. The experimental scenario is shown in Figure 12(a).

B. EXPERIMENTAL PROTOCOL DESIGN

On the one hand, to verify the accuracy of the mmWave radar model proposes in this paper to measure the behavioral trajectory of the participants. As in Figure 10(b), a 4m×4m square experimental environment is built in the laboratory, and the intelligent-tracking trolley is required to follow the route planned on the ground. The difference between the measured trajectory of the radar and the ground-truth trajectory is analyzed by comparing the trajectory of the intelligent-tracking trolley recorded by the mmWave radar. On the other hand, a clinical experiment protocol is designed to validate the quantitative fall risk assessment system proposed in this paper. Participants are recruited to participate in the experiment. The actual scenario of the participating tests is shown in Fig.10(c). The position of the behavioral trajectories of the participants measured by the mmWave radar in the quantitative assessment experiment is shown in Fig.10(d).

In the quantitative fall risk assessment experiment, participants walk through the experimental scenario in numerical

TABLE 2. Feature parameters that characterize the motor function.

Feature Parameters	Definition
Task execution time T	Defined as the duration of each task.
Centroid trajectory length L	Defined as the total length of the center-of-mass curve over the test time, reflecting the speed of center-of-mass sway.
Trajectory offset D	Defined as the average center-of-mass wobble in the Y-direction, reflecting the center-of-mass position.
Maximum swing diameter R	Defined as the difference between the maximum and minimum values in the Y-direction, reflecting the magnitude of the change in position of the center-of-mass over time.
Envelope area S	Defined as the area encompassed by the trajectory of the center-of-mass, reflecting the sway of the body center-of-mass.
Track length per unit area LA	Defined as the ratio of total trajectory length to envelope area, reflecting the changing trend of human posture.
Average velocity V	Defined as the average of the velocity during a motion.
Pause duration P	Defined as stopping time on the way to perform each task.

order, as in Figure 10(b). Each subject participates in the experimental procedure in three main stages:

Step 1: First, the participant stands still at the starting position for 5 seconds. Second, the participant steps in place and waited for experimental instructions. Then, the participant is asked to complete the specified action at the speed of their normal walking state.

Step 2: The participant walks straight along a planned trajectory, and data on the participant's position, velocity, and acceleration are recorded.

Step 3: The participant walks along a planned trajectory square, and mmWave radar simultaneously records the actual trajectory of the participant's movement.

1) PARTICIPANTS

We recruit several elderly participants with fall risk and healthy young participants to participate in the quantitative assessment experiment on fall risk. In the course of the experiment, in addition to asking the elderly subjects to complete the above steps in a normal state, we also instruct the elderly participants and young participants to simulate the abnormal walking situation to different degrees. Through actual measurement and simulation, we establish 256 sets of sample data, which served as the data basis for the subsequent analysis of the subjects' balance ability. The recruitment criteria for the elderly participants included: a) aged between 65 and 80 years; b) a history of falls; c) healthy elderly individuals with no history of falls and good gait status; d) elderly individuals with good mental status and able to communicate normally.

In this research, we select the "Falls Risk Assessment Scale for Older Adults" from Geriatrics and invite raters to assess the dynamic balance ability of the participants using the Clinical Assessment Scale. The scale is used to determine the trend of the human balance and to predict the risk of falls in older adults.

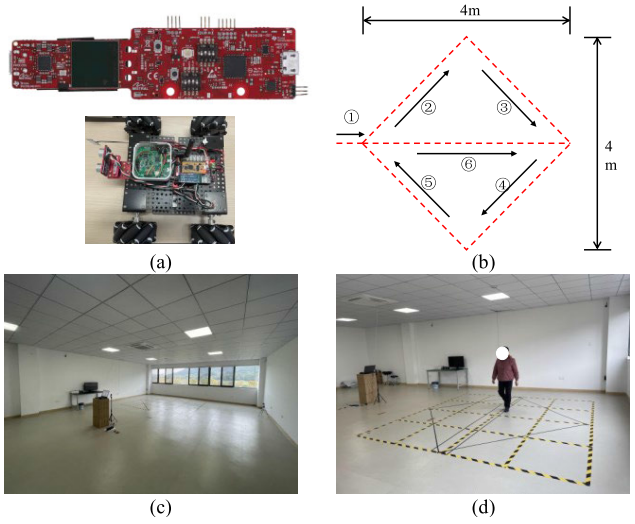

FIGURE 10. Experimental scenarios. (a) Devices. (b) Walking track route. (c) Test scenarios. (d) Elderly trajectory experiment.

2) FEATURE EXTRACTION

Studies of motor performance in elderly participants with balance disorders have identified several metrics to quantify relevant motor functions in participants. Zhang et al. [30] chose velocity metrics, trajectory deviation, and normalized path length to characterize motor motion performance. With reference to the aforementioned relevant studies on motor performance characterization and the professional recommendations of clinicians, eight characteristic motor parameters are selected in this paper. The symbols and definitions of the specific characteristic parameters are shown in Table 2.

a. The length of the centroid trajectory is calculated as follows

$$L = \sum_{i=1}^{N-1} \sqrt{(x_{i+1} - x_i)^2 + (y_{i+1} - y_i)^2} \tag{27}$$

where x_i, x_{i+1} and y_i, y_{i+1} are the coordinates of two neighboring sampling points, and N is the number of sampling points of the trajectory.

b. The trajectory offset is calculated as follows

$$D = \frac{1}{N}\sum_{i=1}^{N}|\Delta D_i| \tag{28}$$

where ΔD_i is the deviation between the real-time trajectory point and the original trajectory's corresponding point.

c. The maximum swing diameter is calculated as follows

$$R = \max\left(\Delta D_i\right) - \min\left(\Delta D_j\right) \tag{29}$$

where ΔD_i is the maximum trajectory offset, and ΔD_j is the minimum trajectory offset.

d. The envelope area is calculated as follows

$$S = \sum_{i=1}^{N}(y_{i+1} - y_i)\sqrt{(x_{i+i} - x_i)^2 + (y_{i+1} - y_i)^2} \tag{30}$$

e. The track length per unit area is calculated as follows

$$LA = \frac{\sum_{i=1}^{N}(y_{i+1} - y_i)\sqrt{(x_{i+i} - x_i)^2 + (y_{i+1} - y_i)^2}}{\sum_{i=1}^{N-1}\sqrt{(x_{i+1} - x_i)^2 + (y_{i+1} - y_i)^2}} \tag{31}$$

f. The average velocity is calculated as follows

$$V = \frac{1}{T}\sum_{i=1}^{N-1}\sqrt{(x_{i+1} - x_i)^2 + (y_{i+1} - y_i)^2} \tag{32}$$

where T is the total time of target motion.

3) MODEL EVALUATION INDEX

The dataset must be divided into training, validation, and test sets in a specific machine-learning model evaluation ratio. The test set is utilized to get the final results after the training is completed to determine the merit of the trained model, but this situation can lead to overfitting of the model on the test set.

In this research, we adopt K-Fold Cross Validation, which can effectively avoid the influence of information leakage on the model's hyperparameters. As shown in Figure 11, firstly, the whole training set is divided into K partitions of the same size according to formula (33). Secondly, different partitions are selected for each partition as the test set in turn, and the remaining K-1 districts are used as the training set. Lastly, the whole process requires training and testing each of the K times, and the results of the K tests are averaged to evaluate the model's effectiveness.

$$\begin{cases} K \approx \ln N \\ N/K > 3d \end{cases} \tag{33}$$

where K is the size of the cross fold, N is the total number of samples in the dataset, and d is the number of feature parameters from Table 2 above.

Ding et al. [28] proposed a prediction model for quantitative evaluation based on a machine learning algorithm in their study of quantitative evaluation methods for motor function.

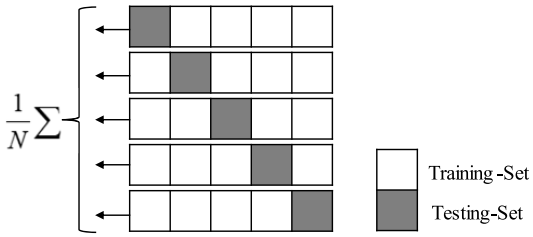

FIGURE 11. Fundamental figure of K-fold cross validation.

The prediction model score in the quantitative evaluation method for the motor function is correct if the absolute value of the difference between the clinician's scale score and the model prediction score is less than or equal to three scores. Therefore, the model prediction is considered accurate if the absolute value of the difference between the clinician's scale score and the score predicted by the model is less than or equal to one score. This research uses four machine learning algorithms to assess the human dynamic balance ability quantitatively. The accuracy, mean absolute error, mean square error, and determination coefficient is used to assess the fitting performance of the model [31].

a. Accuracy is defined as the percentage of the number of samples with absolute error less than one score of the total number of samples in the test set, and the formula is as follows

$$Accuracy = \frac{N_s}{N_t} \times 100\% \tag{34}$$

b. The mean absolute error (MAE) is calculated as follows

$$MAE = \frac{1}{N}\sum_{i=1}^{N}\left|\left(y_i - \hat{y}_i\right)\right| \tag{35}$$

c. The mean square error (MSE) is calculated as follows

$$MSE = \frac{1}{N}\sum_{i=1}^{N}\left(y_i - \hat{y}_i\right)^2 \tag{36}$$

d. The determination coefficient (R^2) is calculated as follows

$$R^2 = 1 - \frac{\sum_{i=1}^{N}\left(y_i - \hat{y}_i\right)^2}{\sum_{i=1}^{N}\left(y_i - \overline{y_i}\right)^2} \tag{37}$$

where N_s is the number of samples with absolute error less than one score, N_t is the total number of samples in the test set, y_i is the physician scale score, $\overline{y_i}$ is the mean of y_i, and $\hat{y}_i$ is the prediction score of the model.

It is also important to note the limitations of our current study. The total sample size of the dataset used to build the evaluation model is 256, and the relatively small sample size in this study may limit the evaluation performance of the model. Therefore, more clinical trials will be needed to collect more data to improve the accuracy of the evaluation model.

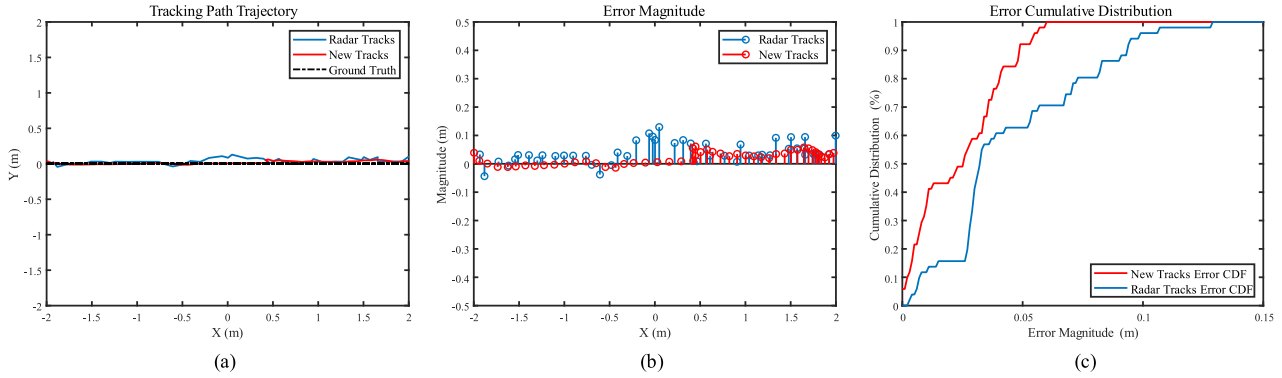

FIGURE 12. Intelligent tracking trolley tracking results. (a) Tracking path diagram. (b) Straight line needle diagram. (c) Errors cumulative distribution.

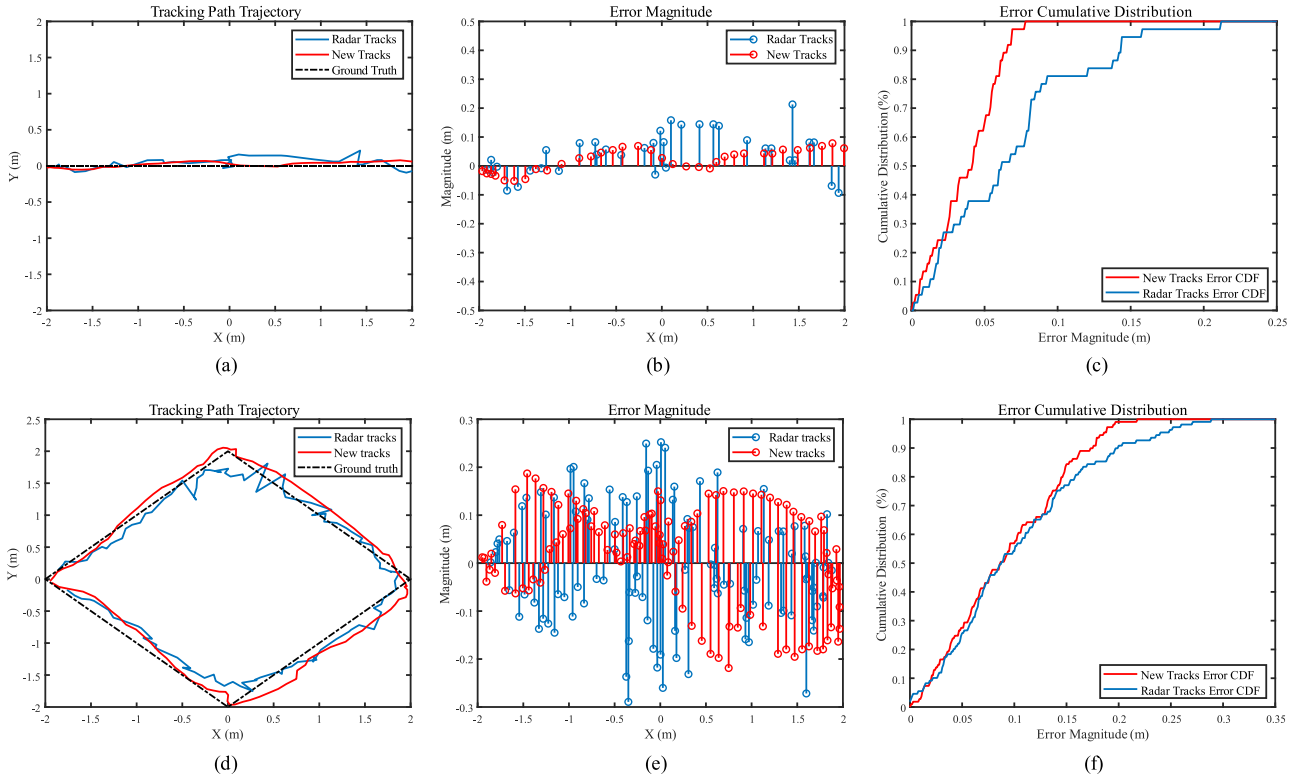

FIGURE 13. Youth people tracking results. (a) Straight line tracking path diagram. (b) Straight line needle diagram. (c) Straight line errors cumulative distribution. (d) Square tracking path diagram. (e) Square line needle diagram. (f) Square errors cumulative distribution.

VI. RESULTS AND DISCUSSION

A. MMWAVE RADAR TRAJECTORY TRACKING PERFORMANCE ANALYSIS

For the mmWave radar-based dynamic trajectory tracking algorithm proposes in this study, the intelligent-tracking trolley travels at a constant speed according to a predetermined track to obtain accurate data. To ensure the accuracy of the collected data, the intelligent-tracking trolley is driven at a speed of 1 m/s along a straight trajectory. Figure 12 shows the tracking results of the intelligent-tracking trolley traveling along a straight line, with the dashed line indicating the ground-truth trajectory, the solid blue line indicating the tracking trajectory before algorithm improvement, and the solid red line indicating the tracking trajectory after algorithm improvement. Figure 12(a) shows the tracking path of the ground-truth trajectory and the tracking trajectories before and after algorithm improvement. In contrast, Figure 12(b) shows the needle diagram of the tracking trajectories and the ground-truth trajectory before and after algorithm improvement. Figure 12(c) shows the analysis of the errors' cumulative distribution for different schemes before and after the algorithm improvement.

As shown in Figure 12, when the intelligent-tracking trolley moves along a straight line, the tracking depicts a minor

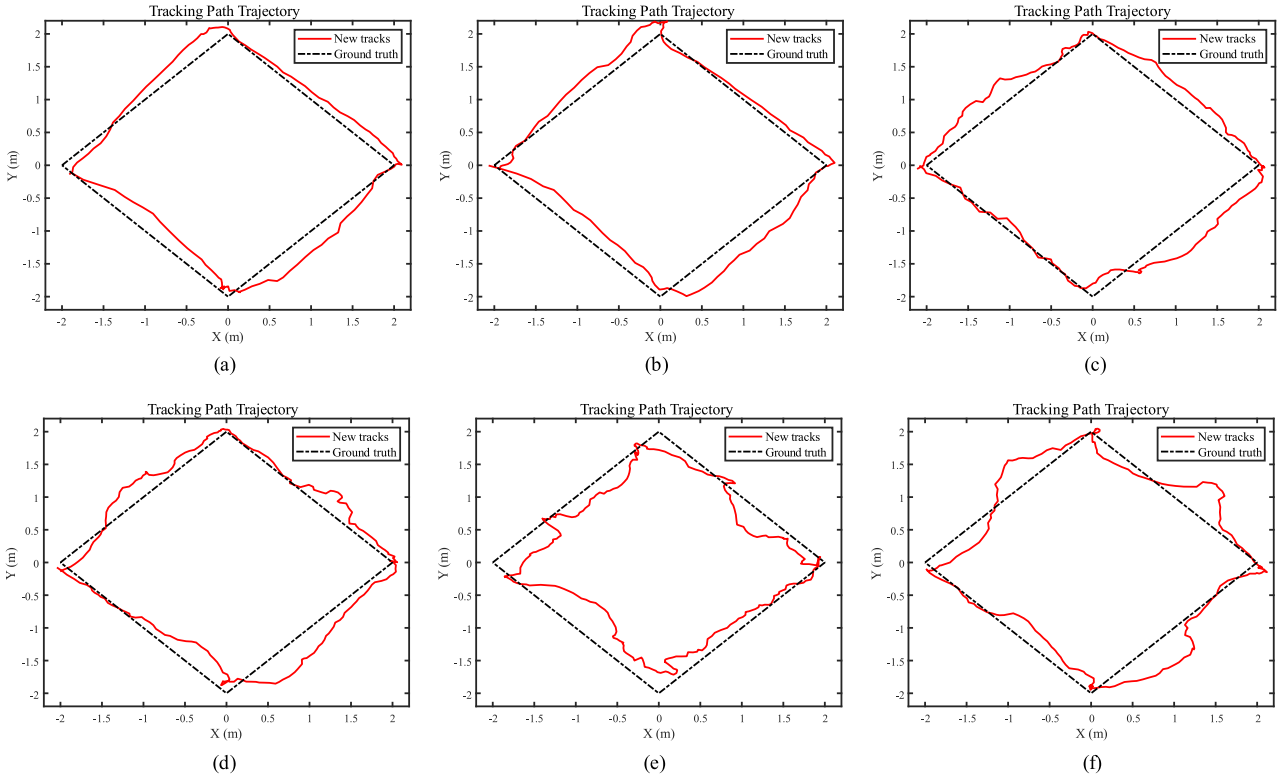

FIGURE 14. Elderly tracking results. (a) 1-score movement. (b) 2-score movement. (c) 5-score movement. (d) 6-score movement. (e) 7-score movement. (f) 8-score movement.

tracking error. The average absolute error of the tracking trajectory for ten experiments before algorithm improvement is 0.04940m, and after algorithm improvement is 0.02879m, indicating more accurate tracking results. From Figure 12(c) above, it can be seen that the algorithm starts to converge at an error of 0.129m before the algorithm improvement. In comparison, the algorithm starts to converge at an error of 0.06m after the algorithm improvement, which shows that the algorithm improvement has been improved. The mmWave radar-based target trajectory tracking accurately depicts the target on a straight trajectory, with the accurate trajectory and tracking trajectory overlapping and the tracking effect reaching the expected accuracy. This method can be applied accurately to track human walking trajectories indoors.

Subsequently, 7 youth people are invited to walk at a constant speed 4 times in the experimental scene according to the digital order shown in Figure 10(b), obtaining 28 sets of straight walking trajectory information and 28 sets of square walking trajectory information. Figure 13 shows the tracking results of young people walking straight and square paths. The dashed line indicates the ground-truth trajectory, the solid blue line indicates the tracking trajectory before algorithm improvement, and the solid red line indicates the trajectory after algorithm improvement.

Figures 13(a)(d) show the tracking path of the ground-truth trajectory and the tracking trajectories before and after algorithm improvement. In contrast, Figure 13(b)(e) shows the tracking trajectories' needle diagram and the ground-truth trajectory before and after algorithm improvement. Figure 13(c)(f) shows the analysis of the cumulative distribution of errors for different schemes of tracking trajectories.

Figure 13 shows that 7 young participants walk along a straight line or a square, and track the depicted trajectories with minor tracking errors. After algorithm optimization, the average experimental error decreases from 2.9455m to 0.3948m. As shown in Figure 13(f) above, the algorithm starts to converge at an error of 0.218m before the algorithm is improved. In comparison, the algorithm starts to converge at an error of 0.289m after the algorithm is improved, with an increase in the average error effect of 9.95%. The above experiments indicate that the algorithm improvement significantly enhances the trajectory tracking and brings it closer to the real human walking trajectory. The experiment of tracking young participants' trajectories confirms the feasibility of tracking indoor human walking trajectories and suggests that the indoor tracking of elderly adults' walking trajectories can reflect their real-time movement trajectories well. Furthermore, recording the elderly participants' movement trajectory during walking, such as speed, centroid trajectory length, and trajectory offset, is of great practical significance.

Finally, in the experiment of quantitative assessment of fall risk, we invite elderly participants with different severity levels to participate in the experiment. They are required to walk in the experimental scenario following the numerical sequence shown in Figure 10(b). Their square walking

trajectories with different clinical scale scores are obtained, as shown in Figure 14.

According to Figure 14, each score's tracking effect in assessing fall risk in older adults can be seen. Figure 14(a) shows the 1-score movement experiment, where elderly participants started slowly. Figure 14(b) shows the 2-score movement experiment, where elderly participants started slowly and turned once obviously. Figure 14(c) shows the 5-score movement experiment, where elderly participants started slowly, turned twice obviously, swayed from side to side in some stages of walking, and stopped twice in the middle. Figure 14(d) shows the 6-score movement experiment, where elderly participants with a disability in the left leg turned twice, walked offline, and stopped once in the middle. Figure 14(e) shows the 7-score movement experiment, where elderly participants with a disability in the right leg turned three times, walked offline, and stopped twice in the middle. Figure 14(f) shows the 8-score movement experiment, where elderly participants with a disability in the left leg turned three times, walked offline, swayed from side to side, and stopped three times in the middle. Figure 14 shows the elderly participants' walking performance, such as not walking straight and long pauses time during turning, which can be observed.

Figure 15 shows the cumulative distribution of errors for different scores in the fall risk assessment experiment for older adults. In the 1-score experiment with lower scores in the fall assessment experiment for older adults, the localization error starts to converge at 0.236m. In comparison, in the 8-score experiment with higher scores, the localization error starts to converge at 0.497m. It can be seen that the localization error is significantly and positively correlated with the scores of older adults in different scores. In short, there is a strong correlation between the effect of trajectory tracking in fall risk assessment experiments for older adults and the scale scores of fall risk assessment.

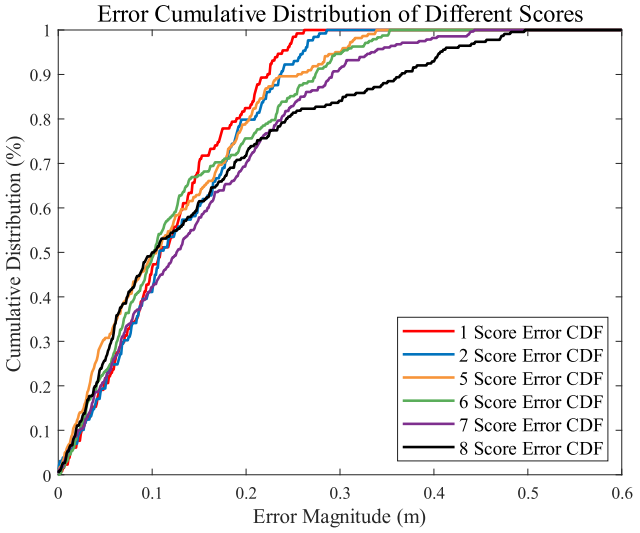

FIGURE 15. Errors cumulative distribution for different scores.

Therefore, the effectiveness of the algorithm improvement in the early stage of this study is significant. The improvement in the tracking effect of the mmWave radar is notable. Applying the elderly participants' kinematic parameters extracted by the mmWave radar to the subsequent quantitative fall risk assessment is also highly meaningful.

B. QUANTITATIVE ASSESSMENT ANALYSIS OF FALL RISK IN OLDER ADULTS

To validate the effectiveness of the quantitative risk assessment method for falls in older adults propose in this study. Pearson correlation analysis is conducted between the motion characteristics and clinical scale scores, as well as between model predicted and clinical scale scores. As shown in Figure 16, the Pearson correlation heatmap shows the correlation strengths between each motion characteristic and clinical scale score. The darker the figure color, the stronger the positive correlation. The lighter the figure color, the stronger the negative correlation. As shown in Figure 16, the correlation between the task execution time and the scale scores is the highest at 0.95, followed by two movement features: average velocity and pause duration. The heatmap shows that the correlation coefficients between the eight motion characteristics proposed in this research and clinical scale scores are all greater than 0.6, indicating that each feature characteristic has a strong correlation and further validating the effectiveness of these characteristics in quantitative risk assessment of falls in older adults.

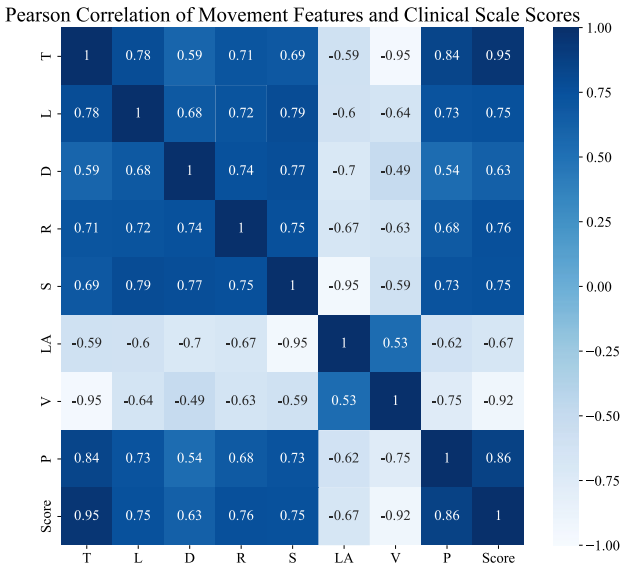

FIGURE 16. Heatmap of Pearson correlation between movement features and clinical scale scores.

The Pearson correlation analysis results between the model predicted, and clinical scale scores are shown in Figure 17. Figure 17(b) shows that the black dots represent the scatter plot of the model predicted and clinical scale scores, while the blue line represents the fitted curve between

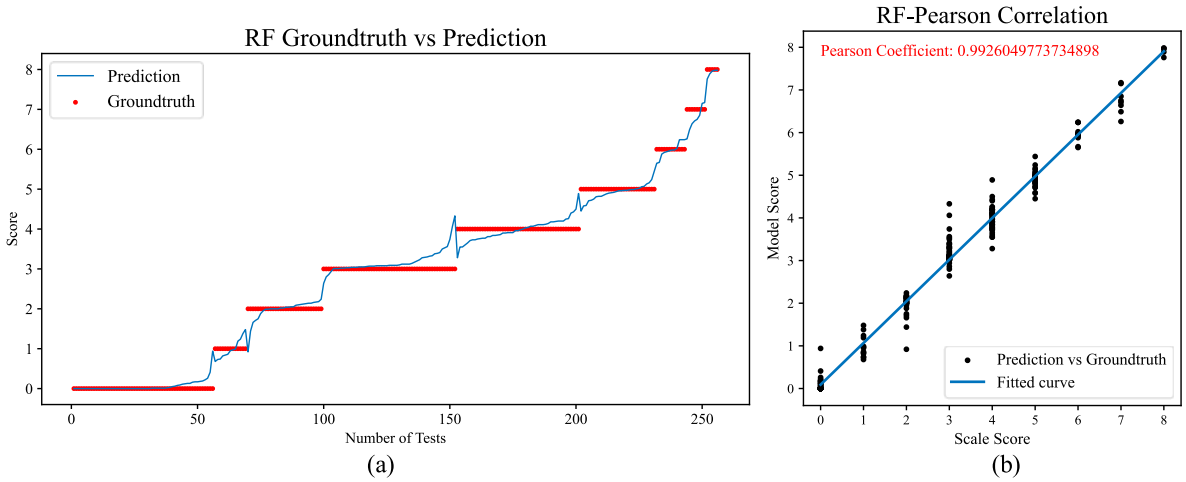

FIGURE 17. Model feature selection. (a) Comparison of model prediction scores and clinical scale scores. (b) RF-Pearson correlation linear analysis.

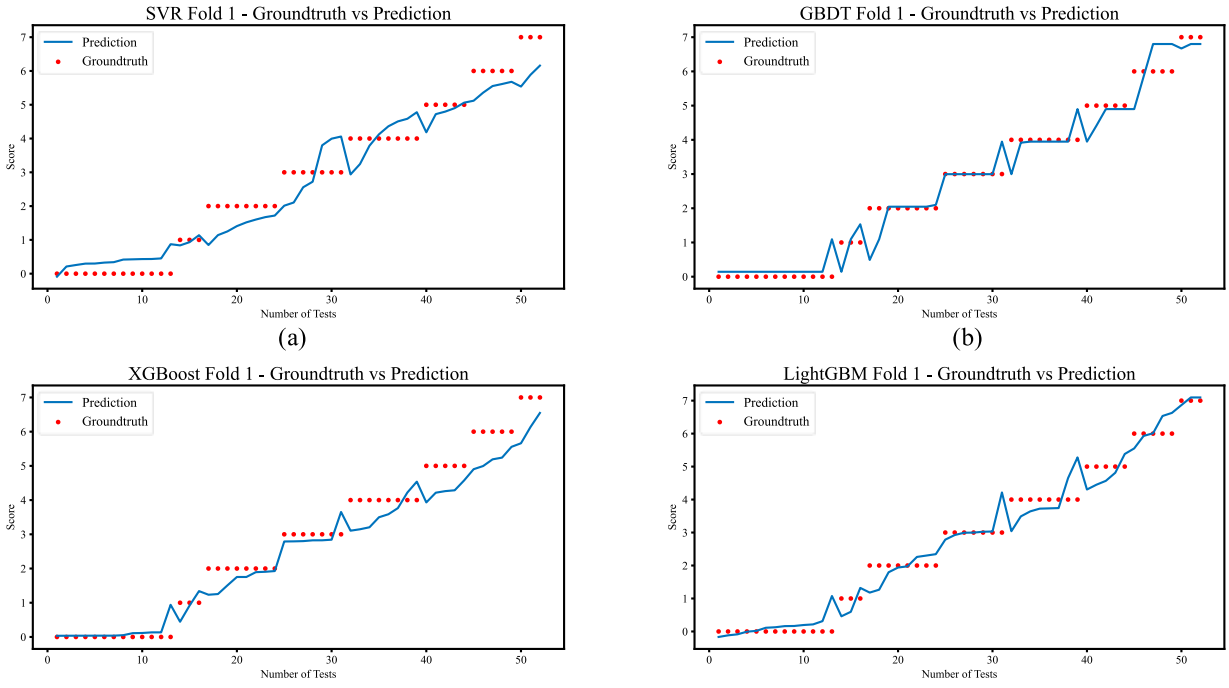

FIGURE 18. Comparison of the prediction score of the four evaluation models with the doctor's scale. (a) SVR. (b)GBDT. (c)XGBoost. (d)LightGBM.

both. The Pearson correlation coefficient between the features uses in the RF model and the clinical scale scores is 0.9926, indicating a linear relationship between the two evaluation methods and proving the significant correlation between the feature selection and clinical scale scores in this study.

The motion feature dataset is used as input to the machine learning quantitative model, and the data are chunked using K-fold cross validation. Since the size of the cross-fold K often receives the influence of various factors, the value of K is generally taken in the interval of [2] and [10]. According to formula (33), the total number of samples N of the data set is 256, thus obtaining $K = 5$ and $d = 8$, which is in line with the parameter selection of this model. The way of dividing the dataset into testing set and training set according to a certain proportion is discarded, thus avoiding the phenomenon of model overfitting on the test set.

With the model metrics above, the dynamic balance ability motor parameters are assessed and analyzed by machine learning to obtain model prediction scores. The predicted scores of the four assessment models based on machine learning algorithms (Fold 1) are compared with the clinical scales as shown in Figure 18. The red scatter plot represents the clinical scale scores, and the blue fitted curve represents the quantitative evaluation model scores for predicted scores.

TABLE 3. 5-fold cross-validation of accuracy results for four assessment models.

Fold	1	2	3	4	5	*Accuracy*
SVR	90.38%	86.27%	80.39%	94.12%	60.78%	82.39%
GBDT	90.38%	86.27%	96.08%	94.12%	92.16%	91.80%
XGBoost	92.31%	92.16%	94.12%	94.12%	90.20%	92.58%
LGBM	94.23%	94.12%	92.16%	94.12%	92.16%	**93.36%**

In the five-fold cross-validation results of the four evaluation models in Table 3, LightGBM's evaluation model predicts the best accuracy performance. As shown in Figure 18 and Table 3, the accuracy, mean absolute error, mean square error and coefficient of determination of the four evaluation models are calculated to compare their performance and verify their effectiveness.

In Table 4, among the four quantitative assessment models based on machine learning algorithms selected in this study, the LightGBM model has the highest prediction accuracy of 93.36%, the smallest mean absolute error of 0.3473, the smallest mean squared error of 0.2454, and the determination coefficient of 0.9404. This shows that the quantitative assessment model based on LightGBM has the best performance in evaluating the human body's dynamic balance capacity performance is the best.

TABLE 4. Comparison of evaluation indexes of four evaluation models.

Index	SVR	GBDT	XGBoost	LGBM
Accuracy	82.39%	91.80%	92.58%	**93.36%**
MAE	0.5741	0.3686	0.3731	**0.3473**
MSE	0.5250	0.2847	0.2847	**0.2454**
R^2	0.8736	**0.9277**	0.9280	0.9404

VII. LIMITATIONS AND FUTURE WORK

This study investigates a quantitative assessment system for evaluating the risk of falls in older adults using 60GHz mmWave radar and machine learning algorithms. The results demonstrate that this system has good predictive performance and can be applied to non-contact monitoring and evaluation of elderly falls [13]. However, there are still some limitations to the proposed method. Firstly, mmWave radar can only track a single object. Multiple mmWave radars can be combined to improve tracking effectiveness to reliably track multiple objects or a single object in complex home environments [32]. Secondly, the sample size of elderly participants tested in the experiment is small. More clinical trials are needed to validate the proposed evaluation model's performance and improve the model prediction and evaluation accuracy. Finally, a Kinect motion sensing device can be used to synchronously capture the skeletal information of the human body to track body movements, and the combination of both can achieve higher accuracy to further comprehensively assess the balance ability and even the tendency of falls in older adults [33].

In future work, more clinical trials will be conducted to improve the performance indicators of the evaluation model and explore a complete elderly health monitoring and evaluation system that combines home monitoring with clinical evaluation. The aim is to promote the intelligent elderly care mode to thousands of households and develop a monitoring and evaluation system for elderly people who live alone, realizing a "Hospital + Family + Elderly" three-in-one smart elderly care mode.

VIII. CONCLUSION

This paper proposes a quantitative assessment system for elderly fall risk based on 60GHz mmWave radar imaging and trajectory feature fusion. The system uses the DBSCAN clustering algorithm with Doppler frequency shift to obtain the center-of-mass position of the human target and the EKF-based human dynamic trajectory prediction algorithm to achieve target tracking. Through Pearson feature correlation analysis and motion feature selection based on RF model, the significant correlation between features and clinical scale scores is determined. Finally, four different machine learning algorithms are used to predict the human dynamic balance ability assessment score to achieve a fine-grained quantitative assessment. Experimental test results show that LightGBM performs the best among the four evaluation models, with a prediction accuracy of 93.36%. The system can be used as an effective means to assist in the daily monitoring of elderly fall risks at home.

REFERENCES

[1] World Health Organization. (2023). *Progress Report on the United Nations Decade of Healthy Ageing, 2021–2023*. [Online]. Available: https://www.who.int/publications/i/item/9789240079694

[2] National Institute on Aging. (2019). *Social Isolation, Loneliness in Older People Pose Health Risks*. [Online]. Available: https://www.nia.nih.gov/news/social-isolation-loneliness-older-people-pose-health-risks

[3] World Health Organization. (2021). *Step Safely: Strategies for Preventing and Managing Falls Across the Life Course*. [Online]. Available: https://www.who.int/publications/i/item/978924002191-4

[4] D. J. J. van Gulick, S. I. B. Perry, M. van der Leeden, J. G. M. van Beek, C. Lucas, and M. M. Stuiver, "A prediction model for falls in community-dwelling older adults in podiatry practices," *Gerontology*, vol. 68, no. 11, pp. 1214–1223, 2022.

[5] X. Zeng, H. S. L. Báruson, and A. Sundvall, "Walking step monitoring with a millimeter-wave radar in real-life environment for disease and fall prevention for the elderly," *Sensors*, vol. 22, no. 24, p. 9901, Dec. 2022.

[6] J. Howcroft, J. Kofman, and E. D. Lemaire, "Prospective fall-risk prediction models for older adults based on wearable sensors," *IEEE Trans. Neural Syst. Rehabil. Eng.*, vol. 25, no. 10, pp. 1812–1820, Oct. 2017.

[7] M. M. Manuel, K. Nellie, and O. Abdelhady, "Evaluation of clinical practice guidelines on fall prevention and management for older adults," *JAMA Netw. Open*, vol. 4, no. 12, Dec. 2021, Art. no. e2138911.

[8] National Institute for Health and Care Excellence. (2013). *Falls in Older People: Assessing Risk and Prevention*. [Online]. Available: https://www.nice.org.uk/guidance/cg161/chapter/Introduction

[9] M. M. Lusardi, S. Fritz, A. Middleton, L. Allison, M. Wingood, E. Phillips, M. Criss, S. Verma, J. Osborne, and K. K. Chui, "Determining risk of falls in community dwelling older adults: A systematic review and meta-analysis using posttest probability," *J. Geriatric Phys. Therapy*, vol. 40, no. 1, pp. 1–36, 2017.

[10] L. Rocchi, L. Chiari, and A. Cappello, "Feature selection of stabilometric parameters based on principal component analysis," *Med. Biol. Eng. Comput.*, vol. 42, no. 1, pp. 71–79, Jan. 2004.

[11] C. Jaschinski, S. B. Allouch, O. Peters, and J. V. Dijk, "The influence of privacy on the acceptance of technologies for assisted living," in *Proc. Int. Conf. Human-Comput. Interact.*, Jul. 2020, pp. 463–473.

[12] R. N. Ferreira, N. F. Ribeiro, and C. P. Santos, "Fall risk assessment using wearable sensors: A narrative review," *Sensors*, vol. 22, no. 3, p. 984, Jan. 2022.

[13] P. Bet, P. C. Castro, and M. A. Ponti, "Fall detection and fall risk assessment in older person using wearable sensors: A systematic review," *Int. J. Med. Informat.*, vol. 130, Oct. 2019, Art. no. 103946.

[14] D. Berardini, S. Moccia, L. Migliorelli, I. Pacifici, P. D. Massimo, M. Paolanti, and E. Frontoni, "Fall detection for elderly-people monitoring using learned features and recurrent neural networks," *Experim. Results*, vol. 1, p. e7, Feb. 2020.

[15] B.-H. Wang, J. Yu, K. Wang, X.-Y. Bao, and K.-M. Mao, "Fall detection based on dual-channel feature integration," *IEEE Access*, vol. 8, pp. 103443–103453, 2020.

[16] P. Zhao, C. X. Lu, J. Wang, C. Chen, W. Wang, N. Trigoni, and A. Markham, "MID: Tracking and identifying people with millimeter wave radar," in *Proc. 15th Int. Conf. Distrib. Comput. Sensor Syst. (DCOSS)*, May 2019, pp. 33–40.

[17] M. G. Amin, Y. D. Zhang, F. Ahmad, and K. C. D. Ho, "Radar signal processing for elderly fall detection: The future for in-home monitoring," *IEEE Signal Process. Mag.*, vol. 33, no. 2, pp. 71–80, Mar. 2016.

[18] X. Wang, J. Ellul, and G. Azzopardi, "Elderly fall detection systems: A literature survey," *Frontiers Robot. AI*, vol. 7, p. 71, Jun. 2020.

[19] S.-H. Park, "Tools for assessing fall risk in the elderly: A systematic review and meta-analysis," *Aging Clin. Experim. Res.*, vol. 30, no. 1, pp. 1–16, Jan. 2018.

[20] H. GholamHosseini, M. M. Baig, M. J. Connolly, and M. Lindén, "A multifactorial falls risk prediction model for hospitalized older adults," in *Proc. 36th Annu. Int. Conf. IEEE Eng. Med. Biol. Soc.*, Aug. 2014, pp. 3484–3487.

[21] B. R. Greene, S. J. Redmond, and B. Caulfield, "Fall risk assessment through automatic combination of clinical fall risk factors and body-worn sensor data," *IEEE J. Biomed. Health Informat.*, vol. 21, no. 3, pp. 725–731, May 2017.

[22] A. K. Mishra, M. Skubic, L. A. Despins, M. Popescu, J. Keller, M. Rantz, C. Abbott, M. Enayati, S. Shalini, and S. Miller, "Explainable fall risk prediction in older adults using gait and geriatric assessments," *Frontiers Digit. Health*, vol. 4, May 2022, Art. no. 869812.

[23] K. Zhang, W. Liu, J. Zhang, Z. Li, and J. Liu, "A fall risk assessment model for community-dwelling elderly individuals based on gait parameters," *IEEE Access*, vol. 11, pp. 120857–120867, 2023.

[24] Y. Yuan, W. Li, Z. Sun, Y. Zhang, and H. Xiang, "Two-dimensional FFT and two-dimensional CA-CFAR based on Zynq," *J. Eng.*, vol. 2019, no. 20, pp. 6483–6486, Aug. 2019.

[25] H. Cui and N. Dahnoun, "High precision human detection and tracking using millimeter-wave radars," *IEEE Aerosp. Electron. Syst. Mag.*, vol. 36, no. 1, pp. 22–32, Jan. 2021.

[26] S. Jahirabadkar and P. Kulkarni, "Algorithm to determine ε-distance parameter in density based clustering," *Exp. Syst. Appl.*, vol. 41, no. 6, pp. 2939–2946, May 2014.

[27] G. Shan, J. Zhang, Y. Ge, and M. Chen, "A comparative study on the generalization ability of back propagation neural network and support vector machine for tracking tumor motion in radiotherapy," in *Proc. 2nd Int. Conf. Biomed. Eng. Bioinf.*, Sep. 2018, pp. 85–88.

[28] K. Ding, B. Zhang, Z. Ling, J. Chen, L. Guo, D. Xiong, and J. Wang, "Quantitative evaluation system of wrist motor function for stroke patients based on force feedback," *Sensors*, vol. 22, no. 9, p. 3368, Apr. 2022.

[29] G. Ke, Q. Meng, T. Finley, T. Wang, W. Chen, W. Ma, Q. Ye, and T. Y. Liu, "LightGBM: A highly efficient gradient boosting decision tree," in *Proc. Adv. Neural Inf. Process. Syst.*, 2017, pp. 3146–3154.

[30] M. Zhang, J. Chen, Z. Ling, B. Zhang, Y. Yan, D. Xiong, and L. Guo, "Quantitative evaluation system of upper limb motor function of stroke patients based on desktop rehabilitation robot," *Sensors*, vol. 22, no. 3, p. 1170, Feb. 2022.

[31] H. Nguyen, Y. Choi, X.-N. Bui, and T. Nguyen-Thoi, "Predicting blast-induced ground vibration in open-pit mines using vibration sensors and support vector regression-based optimization algorithms," *Sensors*, vol. 20, no. 1, p. 132, Dec. 2019.

[32] X. Huang, J. K. P. Tsoi, and N. Patel, "mmWave radar sensors fusion for indoor object detection and tracking," *Electronics*, vol. 11, no. 14, p. 2209, Jul. 2022.

[33] J. Bertram, T. Krüger, H. M. Röhling, A. Jelusic, S. Mansow-Model, R. Schniepp, M. Wuehr, and K. Otte, "Accuracy and repeatability of the Microsoft Azure Kinect for clinical measurement of motor function," *PLoS ONE*, vol. 18, no. 1, Jan. 2023, Art. no. e0279697.

WEI WANG received the bachelor's degree in electrical engineering and automation from the Nanjing University of Information Science and Technology, in 2021. He is currently pursuing the master's degree with Hohai University. His research interests include quantitative assessment of fall risk in the elderly through the fusion of trajectory features and millimeter-wave radar imaging.

YANXIAO GONG received the bachelor's degree in mechanical engineering from Shanghai Jiao Tong University, in 2022. He is currently pursuing the master's degree with the University of Science and Technology of China. His research interest includes the assessment of daily living activities for elderly people using millimeter-wave radar imaging technology.

HAO ZHANG received the bachelor's degree in electronic information engineering from the Nanjing University of Science and Technology, in 2020, and the master's degree from the Nanjing University of Science and Technology, in 2023. His research interest includes using millimeter-wave radar non-contact detection behavior status of the elderly.

XIAOLING YUAN (Member, IEEE) received the master's and Ph.D. degrees in power systems and automation from Hohai University, Nanjing, China, in 1997 and 2004, respectively. She is currently a Professor with the College of Energy and Electrical Engineering, Hohai University. Her current research interest includes automation system control.

YUNPENG ZHANG received the master's degree in microelectronics from Southeast University and the Ph.D. degree in instrument science from the Changchun University of Science and Technology. Since 2019, he has been the PI of the Intelligent Elderly Care Technology Research Group, Suzhou Institute of Biomedical Engineering and Technology, Chinese Academy of Sciences, leading his team to conduct applied research in the direction of non-contact detection of human biological signals and quantitative assessment of elderly behavioral abilities.